OXFORD UNIVERSITY PRESS | Cerebral Cortex

In vivo Evidence of Reduced Integrity of the Grey-White Matter Boundary in Autism Spectrum Disorder

Journal:	*Cerebral Cortex*
Manuscript ID	CerCor-2016-01194.R1
Manuscript Type:	Original Articles
Date Submitted by the Author:	27-Nov-2016
Complete List of Authors:	Andrews, Derek; Institute of Psychiatry, Psychology and Neuroscience, King's College, London, Forensic and Neurodevelopmental Sciences, and the Sackler Institute for Translational Neurodevelopment Avino, Thomas; University of California Davis, Department of Psychiatry and Behavioural Sciences, M.I.N.D Institute Gudbrandsen, Maria; Institute of Psychiatry, Psychology and Neuroscience, King's College, London, Forensic and Neurodevelopmental Sciences, and the Sackler Institute for Translational Neurodevelopment Daly, Eileen; Institute of Psychiatry, Psychology and Neuroscience, King's College, London, Forensic and Neurodevelopmental Sciences, and the Sackler Institute for Translational Neurodevelopment Marquand, Andre; Radboud Universiteit, Donders Institute for Brain, Cognition and Behaviour; Institute of Psychiatry, Psychology and Neuroscience, King's College London, Centre for Neuroimaging Sciences Murphy, Clodagh; Institute of Psychiatry, Psychology and Neuroscience, King's College, London, Forensic and Neurodevelopmental Sciences, and the Sackler Institute for Translational Neurodevelopment; Bethlem Royal Hospital, National Autism Unit Lai, Meng-Chuan; University of Cambridge, Autism Research Centre, Department of Psychiatry; University of Toronto, Child and Youth Mental Health Collaborative at the Centre for Addiction and Mental Health and The Hospital for Sick Children; National Taiwan University Hospital and College of Medicine, Department of Psychiatry Lombardo, Michael; University of Cambridge, Autism Research Centre, Department of Psychiatry; University of Cyprus, Department of Psychology and Center for Applied Neuroscience Ruigrok, Amber; University of Cambridge, Autism Research Centre, Department of Psychiatry Williams, Steven; Institute of Psychiatry, Psychology and Neuroscience, King's College London, Centre for Neuroimaging Sciences Bullmore, Ed; University of Cambridge, Brain Mapping Unit, Department of Psychiatry Suckling, John; University of Cambridge, Brain Mapping Unit, Department of Psychiatry Baron-Cohen, Simon; University of Cambridge, Autism Research Centre, Department of Psychiatry Craig, Michael; Institute of Psychiatry, Psychology and Neuroscience, King's College London, Department of Forensic and Neurodevelopmental

	Sciences, and the Sackler Institute for Translational Neurodevelopment; Bethlem Royal Hospital, National Autism Unit Murphy, Declan; Institute of Psychiatry, Psychology and Neuroscience, King's College London, Department of Forensic and Neurodevelopmental Sciences, and the Sackler Institute for Translational Neurodevelopment; Bethlem Royal Hospital, National Autism Unit Ecker, Christine; Goethe-University Frankfurt am Main, Department of Child and Adolescent Psychiatry, Psychosomatics and Psychotherapy, Universitätsklinikum Frankfurt am Main; Institute of Psychiatry, Psychology and Neuroscience, King's College London, Department of Forensic and Neurodevelopmental Sciences, and the Sackler Institute for Translational Neurodevelopment
Keywords:	ASD, Freesurfer, Imaging, Lamination, MRI

Title Page

Title: In vivo Evidence of Reduced Integrity of the Grey-White Matter Boundary in Autism Spectrum Disorder

Brief Title: Reduced Integrity of the Grey-White Matter Boundary in ASD

Authors: Derek S. Andrews[a] MSc, Thomas A. Avino[b] PhD, Maria Gudbrandsen[a] MSc, Eileen Daly[a] PhD, Andre Marquand[c,d] PhD, Clodagh M. Murphy[a,e] MBChB, Meng-Chuan Lai[f,g,h] MD PhD, Michael V. Lombardo[f,i] PhD, Amber N.V. Ruigrok[f] PhD, the MRC AIMS Consortium[*], Steven C. Williams[d] PhD, Edward T. Bullmore[j] MBBS PhD, John Suckling[j] PhD, Simon Baron-Cohen[f] PhD, Michael C. Craig[a,e] MBBS PhD, Declan G.M. Murphy[a,e**] MBBS MD, & Christine Ecker[k,a**] PhD

Affiliations:

[a] Department of Forensic and Neurodevelopmental Sciences, and the Sackler Institute for Translational Neurodevelopment, Institute of Psychiatry, Psychology and Neuroscience, King's College London, UK

[b] Department of Psychiatry and Behavioral Sciences, M.I.N.D. Institute, University of California Davis, Sacramento, California, USA

[c] Donders Institute for Brain, Cognition and Behaviour, Radboud University, Nijmegen, Netherlands

[d] Centre for Neuroimaging Sciences, Institute of Psychiatry, Psychology and Neuroscience, King's College, London, UK

[e] National Autism Unit, Bethlem Royal Hospital, South London and Maudsley NHS Foundation Trust, UK

[f] Autism Research Centre, Department of Psychiatry, University of Cambridge, Cambridge, UK

[g] Child and Youth Mental Health Collaborative at the Centre for Addiction and Mental Health and The Hospital for Sick Children, Department of Psychiatry, University of Toronto, Toronto, Canada

[h] Department of Psychiatry, National Taiwan University Hospital and College of Medicine, Taiwan

[i] Department of Psychology & Center for Applied Neuroscience, University of Cyprus, Nicosia, Cyprus

[j] Brain Mapping Unit, Department of Psychiatry, University of Cambridge, UK

[k] Department of Child and Adolescent Psychiatry, Psychosomatics and Psychotherapy, Universitätsklinikum Frankfurt am Main, Goethe-University Frankfurt am Main, Germany

[*] The Medical Research Council Autism Imaging Multicentre Study Consortium (MRC AIMS Consortium) is a UK collaboration between the Institute of Psychiatry, Psychology and Neuroscience at King's College, London, the Autism Research Centre, University of Cambridge, and the Autism Research Group, University of Oxford. The Consortium members in alphabetical order are: Anthony J. Bailey (Oxford), Simon Baron-Cohen (Cambridge), Patrick F. Bolton (IoP), Edward T. Bullmore (Cambridge), Sarah Carrington (Oxford), Marco Catani (IoPPN), Bhismadev Chakrabarti (Cambridge), Michael C. Craig (IoPPN), Eileen M. Daly (IoPPN), Sean C. L. Deoni (IoPPN), Christine Ecker (IoPPN), Francesca Happé (IoPPN), Julian Henty (Cambridge), Peter Jezzard (Oxford), Patrick Johnston (IoPPN), Derek K. Jones (IoPPN), Meng-Chuan Lai (Cambridge), Michael V. Lombardo (Cambridge), Anya Madden (IoPPN), Diane Mullins (IoPPN), Clodagh M. Murphy (IoPPN), Declan G. M. Murphy (IoPPN), Greg Pasco (Cambridge), Amber N. V. Ruigrok (Cambridge), Susan A. Sadek (Cambridge), Debbie Spain (IoPPN), Rose Stewart (Oxford), John Suckling (Cambridge), Sally J. Wheelwright (Cambridge), Steven C. Williams (IoPPN), and C. Ellie Wilson (IoPPN).

[**] These authors contributed equally to the manuscript

Corresponding Author:

Mr. Derek Sayre Andrews, BA MSc

PhD Candidate

Department of Forensic & Neurodevelopmental Science

Institute of Psychiatry, Psychology & Neuroscience

King's College London

PO Box 50

16 De Crespigny Park, Denmark Hill

London, England, SE5 8AF

Email: Derek.Andrews@KCL.ac.uk

Work Phone: 02078485701 (UK)

WORD COUNT: **4045**

FIGURES: **3**

TABLES: **2**

ABSTRACT WORD COUNT: **201**

SUPPLEMENTARY FIGURES: **3**

SUPPLEMENTARY TABLES: **3**

KEY WORDS: ASD, Freesurfer, Imaging, Lamination, MRI

Abstract

Atypical cortical organization and reduced integrity of the grey-white matter boundary have been reported by postmortem studies in individuals with Autism Spectrum Disorder (ASD). However, there are no *in vivo* studies that examine these particular features of cortical organization in ASD. Hence we used structural MRI to examine differences in tissue contrast between grey and white matter in 98 adults with ASD and 98 typically developing controls, to test the hypothesis that individuals with ASD have significantly reduced tissue contrast. More specifically, we examined contrast as a percentage between grey and white matter tissue signal intensities (GWPC) sampled at the grey-white matter boundary, and across different cortical layers. We found that individuals with ASD had significantly reduced GWPC in several clusters throughout the cortex (cluster $p<.05$). As expected, these reductions were greatest when tissue intensities were sampled close to grey-white matter interface, which indicates a less distinct grey-white matter boundary in ASD. Our *in vivo* findings of reduced GWPC in ASD are therefore consistent with prior postmortem findings of a less well-defined grey-white matter boundary in ASD. Taken together, these results indicate that GWPC might be utilized as an *in vivo* proxy measure of atypical cortical microstructural organization in future studies.

Introduction

Autism spectrum disorder (ASD) is a lifelong neurodevelopmental condition characterized by impaired social communication, deficits in social reciprocity, and repetitive and stereotypic behaviors and interests (Wing 1997). These core symptoms typically manifest from early childhood, and are accompanied by developmental differences in brain anatomy and connectivity (for review, see Amaral et al. 2008; Ecker et al. 2015; Lange et al. 2014). For example, prior studies of ASD reported atypical measures of cortical anatomy such as folding, thickness, and surface area (Nordahl et al. 2007; Hyde et al. 2010; Ecker et al. 2013a; Schaer et al. 2013) as well as intra cortical connectivity (Ecker et al. 2013b). However, the causes of these cortical abnormalities in people with ASD are unknown.

There is some evidence to suggest that the cortical differences accompanying ASD may result from atypical neuronal proliferation, migration and maturation (Pinto et al. 2014). For example, some genetic variants associated with ASD encode for genes that regulate these neurodevelopmental processes (Huguet et al. 2013). It has been suggested that these variations may explain post-mortem findings such as irregular cortical lamination, the presence of super-numerous neurons in some layers of the cortex, and poor differentiation of the grey-white matter boundary (for review, see Casanova et al. 2014). For example, histological samples from the superior temporal gyrus (approximate Brodmann area [BA] 21), dorsolateral frontal lobe (BA9) and dorsal parietal lobe (BA7) have shown the grey-white matter boundary to be less distinct in ASD as compared to typically developing (TD) controls (Avino and Hutsler 2010). Thus, there is increasing postmortem evidence for abnormal cell patterning within the grey-white matter boundary in ASD. However, to date no study has investigated differences in the integrity of the grey-white matter boundary in ASD *in vivo* across the whole brain.

Current *in vivo* neuroimaging methods for investigating cortical abnormalities in ASD focus on morphometric features such as cortical thickness (CT), i.e. the closest distance from the

grey-white matter boundary to the grey-cerebrospinal fluid (CSF) boundary (Fischl and Dale 2000). Differences in CT have been reported in children, adolescents and adults with ASD, and include regional increases and decreases that may mediate some of the behavioral deficits typically observed in the disorder (Hardan et al. 2006; Hyde et al. 2010; Ecker et al. 2013b). However, measures of CT rely on the accurate delineation of grey and white matter and therefore may be confounded by intrinsic histological abnormalities at the grey-white matter boundary in ASD (Avino and Hutsler 2010).

Hence, we investigated between-group differences related to cortical lamination in both adult males and females with ASD, and matched typically developing (TD) controls, using a whole brain quantitative approach that estimated integrity of the grey-white matter boundary. Namely, we examined the percent contrast of grey-to-white matter signal intensities (GWPC), sampled across different cortical layers in a continuous fashion. Here, the GWPC calculation we employed in the current manuscript is comparable to the grey-white contrast ratio (GWR) as originally reported by Salat et al. (2009). We hypothesized the grey-white matter boundary to be less defined and therefore GWPC to differ significantly in individuals with ASD.

Materials and Methods

Participants

Overall, 98 right-handed adults with ASD (49 males & 49 females) and 98 age, sex, and IQ matched TD controls (51 males & 47 females) aged 18-42 years were recruited by advertisement and assessed at the Institute of Psychiatry, Psychology and Neuroscience (IoPPN), London, and the Autism Research Centre, Cambridge. Approximately equal ratios of cases to controls, and males to females, were recruited within sites (Table 1). Exclusion criteria included a history of major psychiatric disorder (e.g. psychosis), head injury, genetic disorder associated with autism (e.g. fragile-X syndrome, tuberous sclerosis), or any other medical condition affecting brain function (e.g. epilepsy), or any participants taking antipsychotic medication, mood stabilizers or benzodiazepines.

ASD diagnosis was made by a consultant psychiatrist using ICD-10 research diagnostic criteria and confirmed using the Autism Diagnostic Interview–Revised (ADI-R; Lord et al. 1994). ADI-R's were completed for 94 individuals with ASD (49 males & 45 females). 93 (49 males & 44 females) reached algorithm cut-offs for autism in all domains of the ADI-R (social, communication, restricted/stereotyped), although failure to reach cut-off in one domain by one point was permitted. The ADI-R rather than Autism Diagnostic Observation Schedule (ADOS; Lord et al. 2000) was employed as inclusion criteria to ensure that all participants with ASD met the criteria for childhood autism. We were unable to complete ADI-Rs for four females with ASD as their parents/caregivers were not available. However, all four reached algorithm cut-offs for "autism spectrum" on the ADOS (communication, social) diagnostic algorithm. In all other participants, ADOS scores were used to measure current symptoms and not as inclusion criterion. One ASD female scored one point below cut-off for autism on the communication and repetitive behavior domains of the ADI-R but met ICD-10 criteria for ASD and scored above cut-off for "autism" on the ADOS. Overall intellectual ability was assessed using the Wechsler Abbreviated Scale of Intelligence (WASI; Wechsler 1999). All participants had a full-scale IQ greater than 80 and gave informed written consent in accordance with ethics approval by the National Research Ethics Committee, Suffolk, UK.

Structural MRI Data Acquisition

Scanning was performed at the IoPPN, London, and the Addenbrooke's Hospital, Cambridge, using a 3T GE Signa System (General-Electric, Milwaukee, USA). A specialized acquisition protocol using quantitative T1-mapping was used to ensure standardization of structural MRI scans across scanner platforms. This protocol has previously been validated and extensively described elsewhere (Deoni et al. 2008; Ecker et al. 2012), resulting in high-resolution structural T1-weighted inversion-recovery images, with 1x1x1mm resolution, a 256x256x176 matrix, TR=1800ms, TI=50ms, FA=20", and FOV=5cm.

Cortical Reconstruction using FreeSurfer

Previous histological studies have largely relied upon manual identification to define the boundary between grey and white matter. For example, Avino and Hutsler (2010) used a sigmoid function to quantify the distinctiveness of the transition between grey and white matter in Nissl stained histological images. In the current study, however, we employed an automated analytical pipeline using Freesurfer v5.3.0 software (http://surfer.nmr.mgh.harvard.edu/) to identify the grey-white matter boundary by deriving models of the cortical surface for each T1-weighted image. These well-validated and fully automated procedures have been detailed elsewhere (Fischl and Dale 2000; Dale et al. 1999; Fischl et al. 1999; Ségonne et al. 2004; Jovicich 2006). In brief, a single filled white-matter volume was generated for each hemisphere after intensity normalization, extra-cerebral tissue was cropped, and image segmentation performed using a connected components algorithm. A triangular tessellated surface was then generated for each white-matter volume. Deformation of this tessellated white matter surface resulted in a cortical mesh for the surfaces that define the boundary between grey and white matter (i.e. white matter surface), and grey matter and cerebral spinal fluid (CSF) (i.e. pial surface). This surface deformation is the result of the minimization of an energy functional that utilizes intensity gradients in order to place these surfaces where the greatest shift in intensity defines the transition between tissue classes (Dale et al. 1999, Supplementary Materials). The use of intensity gradients across tissue classes assures that boundary placement is not reliant solely on absolute signal intensity and allows for sub voxel resolution in the placement of these boundary surfaces (Dale et al. 1999; Dale and Sereno 1993; Fischl and Dale 2000). These automated methods have previously been validated against histological analyses and have shown a high degree of accuracy in placing the grey-white matter boundary (Rosas et al. 2002). The resulting surface models were visually inspected for reconstruction errors. Participant's surface reconstructions with visible inaccuracies were excluded and are not described in this study. Dropout rates due to

surface reconstruction errors were equal between groups and represented <10% of the total sample.

Grey to White Matter Percent Contrast (GWPC) and Grey Matter Signal Intensity Measures

Grey matter tissue intensities (GMI) were sampled continuously across different cortical layers from the grey-white matter boundary (i.e. white matter surface) to the pial surface. These signal intensities were sampled at different percentile fractions of the total orthogonal distance projected from the white matter to pial surfaces (i.e. projection fractions). Starting at the white matter surface, sampling continued at projection fraction intervals of 10% up to 60% of the distance from the white matter to the pial surface, thus yielding a set of six GMI measures (i.e. from 10 to 60%; Figure 1). The outer 40% (i.e. 70-100%) of the cortical sheet was not sampled in order to assure that sampling was performed within the cortical grey matter, and not confounded by voxels composed of cerebrospinal fluid (CSF). White matter signal intensity (WMI) was measured at 1.0mm into the white matter from the white matter surface (Figure 1). Previously reported measures of tissue contrast have used a ratio calculation (i.e. GMI/WMI; Salat et al. 2009), where larger values indicate a reduced contrast. Here, however, we utilized the formula provided by Freesurfer to calculate tissue contrast as the percentage of GMI at projection fraction (*i*) to WMI at each cerebral vertex (*j*),

$$GWPC_{ij} = 100 * (WMI_{i,1.0mm} - GMI_{i,j}) / 0.5 * (WMI_{i,1.0mm} + GMI_{i,j})$$

Thus, by definition, a decrease in GWPC is commensurate with a decrease in contrast between the grey matter tissue intensity measured at projection fraction *i*, and the white matter tissue intensity measured at 1.0mm subjacent to the white matter surface. We also examined the tissue contrast when sampling GMI at the grey-white matter boundary (i.e. at the white matter surface, projection fraction=0%). The resulting GWPC, GMI, and WMI measures were subsequently smoothed using a 10mm FWHM surface based Gaussian kernel prior to statistical analyses. We also examine between-group comparisons using a 5mm FWHM smoothing kernel, which are shown in Supplementary Figure 3 and Table 3.

Statistical Analyses

Vertex-wise statistical analysis of GWPC, GMI, and WMI measures (Y) were estimated by regression of a general linear model (GLM) with (1) diagnostic group, sex, and acquisition site as categorical fixed-effects factors, (2) a group by sex interaction term, and (3) age and full scale IQ as continuous covariates:

$$Y_i = \beta_0 + \beta_1 Group + \beta_2 Sex + \beta_3[Group \times Sex] + \beta_4 Site + \beta_5 Age + \beta_6 FSIQ + \varepsilon_i$$

where ε_i is the residual error at vertex i. Between-group differences were estimated from the corresponding coefficient β_1, normalized by the corresponding standard error. Our model was selected *a priori* in order to be comparable to previously published research findings based on our sample (Ecker et al. 2013b). Corrections for multiple comparisons across the whole brain were performed using 'random field theory' (RFT)-based cluster analysis for non-isotropic images using a cluster based significance threshold of $p<0.05$ (2-tailed; Worsley et al. 1999). Initially, we investigated between-group differences in GWPC at different grey-matter projection fractions. Subsequently, we also investigated between-group differences in grey and white matter tissue intensities, which allowed us to determine whether the between-group differences in GWPC were driven by differences within the cortical grey or white matter. Last, between-group differences in CT were examined using the same GLM as described above in order to determine how differences in GWPC might affect variability in CT in ASD.

Results

Participant demographics and global brain measures

There were no significant differences between individuals (males and females) with ASD and TD controls in age ($t(194)=-0.53$, $p=0.598$), full-scale IQ ($t(194)=-1.72$, $p=0.086$), or total GM volume ($t(194) = -0.20$, $p=0.839$). There were also no significant differences between males and females in age ($t(194)=-0.93$, $p=0.356$) or full-scale IQ ($t(194)=-1.87$, $p=0.063$). As expected, total grey matter volume in males was significantly larger than in females

($t(194)=9.11$, $p<0.001$). However, there were no significant differences in any of these measures between males with ASD and male controls, or females with ASD and female controls ($p<0.05$, 2-tailed).

Between-group difference in GWPC across the cortex

We initially examined vertex-wise between-group differences in GWPC at different projection fractions into the cortical sheet. At all sampling depths, we found that individuals with ASD had a significantly decreased GWPC in several clusters across the cortex, which is consistent with a reduced tissue contrast between grey and white matter (Figure 2). In accordance with our hypothesis, the reductions in GWPC were most extensive when GMI was sampled at grey-white matter boundary (i.e. the white matter surface, projection fraction=0%), and gradually decreased in both statistical effect and spatial extent with increasing projection fractions into cortex and away from the grey-white matter boundary. Regions where ASD individuals had reduced GWPC as compared to TD controls included the; 1) bilateral posterior cingulate (BA 23/30), medial frontal (BA10) fusiform/entorhinal (BA 34/37) and the inferior and superior temporal cortices (BA20/21/22); 2) left orbitofrontal cortex (BA 11/25) and temporo-parietal junction (BA 39/40); and (3) right dorsolateral prefrontal cortex (BA11/45). Statistical details for all clusters are listed in Table 2. There were no brain regions where individuals with ASD had a significantly increased GWPC relative to controls. The pattern of reduced GWPC among individuals with ASD remained significant when total brain volume or mean cortical thickness were included as covariates. Furthermore, there was minimal spatial overlap between the pattern of differences in GWPC and CT (see supplementary Figure 1 and Table 1).

Between-group differences in grey and white matter tissue intensities

To identify whether the observed differences in GWPC were driven by differences in grey or white matter, or a combination of both, we subsequently examined between-group differences

in both GMI and WMI. Individuals with ASD had significantly increased GMI across all six different GMI sampling depths relative to controls in regions where we also observed decreases in GWPC (Figure 3). These included (1) the bilateral anterior temporal lobes (BA 38/30) and the left middle temporal gyrus (BA 21), (2) the right temporo-parietal junction (BA39/40), and (3) the bilateral fusiform and entorhinal cortex (BA 36). Statistical details for these clusters are listed in Table 1. We did not observe any significant between-group differences in GMI at the grey-white matter boundary (i.e. the white matter surface), or in WMI at 1.0mm within the white matter (Figure 3). There were no brain regions where individuals with ASD had significantly decreased GMI relative to controls. Hence GWPC reductions in ASD were driven predominantly by increased (i.e. brighter) tissue intensities within the cortical grey matter.

Main Effects of Sex and Group by Sex Interactions

Last, we investigated whether biological sex significantly modulates differences in GWPC in ASD by examining group-by-sex interactions. Overall, regardless of diagnosis males had a significantly greater GWPC than females (supplementary Figure 2). This occurred across all sampling depths, and was predominantly in fronto-parietal regions of the left hemisphere, and in bilateral inferior temporal regions (see supplementary Table 2 for statistical details of these clusters). However, there were no brain regions where we observed significant group-by-sex interactions for GWPC. Thus, while males tended to have a significant increase in contrast between grey and white matter tissue intensities, and hence a better defined grey-white matter boundary, the reductions in GWPC that we observed in the brain in individuals with ASD were not explained by biological sex.

Discussion

Our aim was to determine if previous postmortem reports of poor definition of the grey-white matter boundary in ASD could be detected using a whole brain *in vivo* MRI approach. As hypothesized, we determined that individuals with ASD had a significantly less well-defined

tissue contrast (i.e. GWPC) between grey and white matter at (and around) the grey-white matter boundary. The affected brain regions included the superior temporal gyrus (BA21), the dorsolateral frontal lobe (BA9), and the dorsal parietal lobe (BA7) where histological abnormalities in the transition from grey to white matter have also been reported (Avino and Hutsler 2010). The concordance between the regional pattern and direction of the GWPC differences in our sample with previous histological investigations in post mortem brain tissue supports the biological plausibility of our results. Thus, our findings agree with previous postmortem histological studies and indicate that tissue contrasts across the grey-white matter interface may serve as a potential *in vivo* proxy measure for atypical organization of the cortical sheet in ASD.

Prior postmortem studies reported abnormalities in the cortical microstructure of individuals with ASD. For example, the boundary between cortical layer VI and underlying white matter has been shown to be significantly less well defined due to increased dispersion of neuronal cells across this interface (Avino and Hutsler 2010). It has been suggested that this may be caused by the presence of supernumerary neurons beneath the cortical plate that arise from disrupted migratory processes or improper resolution of the cortical subplate (Chun and Shatz 1989; Kemper 2010; Hutsler and Avino 2015). The cortical subplate is a transient neurodevelopmental zone that is instrumental in establishing early proper cortical connectivity. Specifically, subplate neurons pioneer the corticothalamic axon pathway, serve as a 'signpost' for cortical afferents, drive endogenous oscillatory activity in the cortex, and act as a transient synaptic hub for thalamocortical axons before they directly innervate the cortical plate (McConnell et al., 1994; Ghosh et al., 1990; Luhmann et al., 2009; Shatz & Luskin, 1986). The maximal volume of the subplate is reached around 30 gestational weeks in the human coinciding with the growth of long-range cortico-cortico projections (Vasung et al., 2016). After their early neurodevelopmental role is complete, a large number of these subplate neurons undergo apoptosis. However, a small percentage of these neurons persist

and retain their connections with the overlying cortical plate acting as modulators of cortical afferents (Chun and Shatz 1989; Dupont et al., 2006; Kostovic et al., 2011).

Therefore, perturbations to early subplate development may disrupt the establishment of structural and functional brain connectivity, which is abnormal in individuals with ASD (Just et al., 2004; Belmonte et al. 2004; Courchesne and Pierce 2005; Balardin et al., 2015). In addition, the abnormal persistence of these neurons after the large wave of programmed cell death could cause disruptions to cortical communication through their modulatory role of the overlying cortex. In this way, the abnormal persistence of subplate neurons into adulthood has been demonstrated in schizophrenia and seizure disorder and is hypothesized to contribute to the pathophysiology of these conditions (Eastwood & Harrison, 2003, 2005; Yang et al., 2011; Andres et al., 2004; Hildebrandt et al., 2005; Kostovic et al. 2011). Furthermore, a recent genetic study reported a set of subplate-specific genes that are associated with ASD (Hoerder-Suabedissen et al. 2013). Thus, there is converging evidence to suggest that neurons of the cortical subplate contribute to the aberrant neuropathology of ASD and that atypical laminar organization, particularly around the grey-white matter boundary, may be a defining characteristic of the condition. However this has never previously been examined *in vivo*.

Thus, in this *in vivo* study we sought to examine differences in cortical lamination and grey-white matter boundary integrity in ASD. To achieve this we measured contrasts between grey and white matter tissue intensities (GWPC; Salat 2009). These MRI measures were taken at the interface of grey and white matter and across cortical layers at six different depths into the cortical sheet from the grey-white matter boundary (i.e. white matter surface). In our ASD cases many regions with reduced GWPC also showed significantly increased GMI but no differences in WMI as compared to TD controls. This suggests (in agreement with prior *in vivo* work by our group; Ecker 2016) that ASD may be primarily associated with disruptions to cortical grey matter as opposed to white matter. This increased GMI in ASD may result from atypical myelination (Sowell et al. 2004) and/or atypical cytoarchitectural organization

such as greater numbers of more densely packed cortical minicolumns (Casanova et al. 2006) and reductions in grey level amplitude in these structures (Casanova et al. 2002).

The regional specificity of our findings of decreased tissue contrast may be related to the differential expansion of the subplate between cortical areas. Evolutionarily, the size and complexity of the subplate is most prominent in humans as it accommodates the increased connectivity with cortical and subcortical areas relative to non-human primates and rodents (Kostovic & Rakic, 1990; Judas et al., 2013). Within humans, the subplate zone is larger in cortical association areas as a consequence of the increased number of axons invading these regions. These incoming axons displace subplate neurons deeper into the white matter, which occurs to a greater degree in these association areas (Duque et al., 2016). Atypicalities at the grey-white matter interface may therefore impact on MRI intensity values, and may explain the regional specificity observed in our pattern of results. Moreover, the regional pattern of GWPC seems to be linked to the functional deficits that are characteristic for ASD. For example, we observed deficits in GWPC in several regions mediating social processing and wider socio-cognitive functioning, including the insula, fusiform gyrus, cingulate cortex, middle temporal gyrus, superior temporal sulcus, and prefrontal cortical regions (see Just et al. 2012 for review). Thus, while future studies are required to establish the functional relevance of our results directly, it is likely that atypical GWPC contributes to the cluster of clinical symptoms typically observed in ASD.

Findings from this and other studies detailing poor delineation of the grey-white boundary in ASD may be taken by some to call into question the accuracy of *in vivo* MRI measures such as CT that rely on the placement of a discrete boundary between grey and white matter. However, the spatially distributed patterns of group-differences in CT we detected did not significantly overlap with the pattern of differences in GWPC (see supplementary Figure 1). Also, including individual's global mean CT as a covariate did not significantly alter the pattern of differences in GWPC. Therefore, while we were able to detect subtle differences in

tissue contrast in ASD, at the level of spatial resolution neuroimaging techniques currently offer, these do not appear to be large enough to significantly affect estimates of CT within our sample of adults with ASD. This finding is also in agreement with a recent twin study showing that while both GWPC and CT are highly heritable, they have little shared genetic variance (Panizzon et al. 2012). Taken together, these findings suggest that GWPC characterizes additional cortical structural properties that are distinct to CT. Nevertheless, inter-individual differences in the ability to delineate the grey-white matter boundary should be considered in the future when interpreting neuroanatomical features that are based on clearly delineating grey and white matter.

Our study is not without limitations. For instance we examined neuroanatomical differences associated with ASD in adulthood. This, and the cross-sectional nature of our study, inherently limits our ability to draw conclusions on the aetiological and neurodevelopmental basis of the atypical neural structure we observed. However, within our sample, all but four females with ASD met ADI-R criteria for childhood autism. It is therefore likely that the observed pattern of neuroanatomical differences in GWPC may have evolved as a consequence of meeting ASD criteria during early childhood and might therefore be causally related to the condition. Further longitudinal studies will, however, be required to disentangle GWPC differences associated with primary neuropathology from atypical neurodevelopmental trajectories or secondary compensatory mechanisms. Recent work has quantified the volume of transient neurodevelopmental zones in the postmortem human fetal brain using MRI as they relate to major neurogenic events (Vasung et al. 2016). Such information provides a reference for studying early prenatal deviations from typically developing brain growth and could be used in the future to inform *in vivo* imaging. We are further limited by the current resolution of structural MRI images (1mm isotropic voxels). At this resolution it is not possible for us to distinguish between different aspects of cortical cytoarchitecture or accurately delineate particular layers of the cortical sheet as defined by histological staining. Rather, our sampling approach was based on the geometric criteria of

projection fraction percentages into the cortical sheet from the white matter surface (Salat et al. 2009). Furthermore, additional research will be required to elucidate the functional relationship between deficits in GWPC and autistic symptoms and traits.

Taken together, our findings suggest that measures of GWPC sampled across cortical layers may serve as an *in vivo* proxy measure for irregular microstructural organization of the cortex in ASD (and other disorders). Such novel *in vivo* measures that are indicative of atypical cortical organization might in the future be used to stratify the condition, and/or to examine the neuropathology of ASD in particular genetic subgroups known to be linked to specific neurodevelopmental deficits.

Acknowledgements: We would like to thank all of our participants and their family members for partaking in this study. The Autism Imaging Multicentre Study Consortium, members in alphabetical order are: Anthony J. Bailey (Oxford), Simon Baron-Cohen (Cambridge), Patrick F. Bolton (IoP), Edward T. Bullmore (Cambridge), Sarah Carrington (Oxford), Marco Catani (IoPPN), Bhismadev Chakrabarti (Cambridge), Michael C. Craig (IoPPN), Eileen M. Daly (IoPPN), Sean C. L. Deoni (IoPPN), Christine Ecker (IoPPN), Francesca Happé (IoPPN), Julian Henty (Cambridge), Peter Jezzard (Oxford), Patrick Johnston (IoPPN), Derek K. Jones (IoPPN), Meng-Chuan Lai (Cambridge), Michael V. Lombardo (Cambridge), Anya Madden (IoPPN), Diane Mullins (IoPPN), Clodagh M. Murphy (IoPPN), Declan G. M. Murphy (IoPPN), Greg Pasco (Cambridge), Amber N. V. Ruigrok (Cambridge), Susan A. Sadek (Cambridge), Debbie Spain (IoPPN), Rose Stewart (Oxford), John Suckling (Cambridge), Sally J. Wheelwright (Cambridge), Steven C. Williams (IoPPN), and C. Ellie Wilson (IoPPN). The EU-AIMS Consortium. Furthermore, we would like to thank the National Institute for Health Research Biomedical Research Centre for Mental Health, the Dr. Mortimer and Theresa Sackler Foundation, and the German Research Foundation (DFG).

Funding: This work was supported by funded by Medical Research Council UK (grant number G0400061); the Innovative Medicines Initiative Joint Undertaking (grant number 115300), which includes financial contributions from the EU Seventh Framework Programme (FP7/2007-2013) from the European Federation of Pharmaceutical Industries and Associations companies in kind; and from Autism Speaks.

Statement of Disclosure: Professor Edward Bullmore is employed half-time by GlaxoSmithKline and holds GSK shares. Dr. Meng-Chuan Lai receives financial support from the O'Brien Scholars Program within the Child and Youth Mental Health Collaborative at the Centre for Addiction and Mental Health and The Hospital for Sick Children, Toronto. None of the remaining authors have declared any conflict of interest or financial interests, which may arise from being named as an author on the manuscript.

References

Amaral DG, Schumann CM, Nordahl CW. 2008. Neuroanatomy of autism. Trends in neurosciences 31:137-145.

Andres M, Andre V, Nguyen S, Salamon N, Cepeda C, Levine MS, Leite JP, Neder L, Vinters HV, Mathern GW. 2005. Human cortical dysplasia and epilepsy: An ontogenetic hypothesis based on volumetric MRI and NeuN neuronal density and size measurements. Cerebral cortex 15:194-210.

Avino TA, Hutsler JJ. 2010. Abnormal cell patterning at the cortical gray–white matter boundary in autism spectrum disorders. Brain Research 1360:138-146.

Balardin JB, Comfort WE, Daly E, Murphy C, Andrews D, Murphy DG, Ecker C, MRC AIMS Consortium, Sata J. 2015. Decreased centrality of cortical volume covariance networks in Autism Spectrum Disorders. Journal of Psychiatric Research 69:142-149.

Belmonte MK, Allen G, Beckel-Mitchener A, Boulanger LM, Carper RA, Webb SJ. 2004. Autism and abnormal development of brain connectivity. The Journal of Neuroscience 24:9228-9231.

Casanova MF. 2014. Autism as a sequence: from heterochronic germinal cell divisions to abnormalities of cell migration and cortical dysplasias. Medical hypotheses 83:32-38.

Casanova MF, Buxhoeveden DP, Switala AE, Roy E. 2002. Neuronal density and architecture (gray level index) in the brains of autistic patients. Journal of child neurology 17:515-521.

Casanova MF, van Kooten IA, Switala AE, van Engeland H, Heinsen H, Steinbusch HW, Hof PR, Trippe J, Stone J, Schmitz C. 2006. Minicolumnar abnormalities in autism. Acta neuropathologica 112:287-303.

Chun JJM, Shatz CJ. 1989. Interstitial cells of the adult neocortical white matter are the remnant of the early generated subplate neuron population. Journal of Comparative Neurology 282:555-569.

Courchesne E, Pierce K. 2005. Why the frontal cortex in autism might be talking only to itself: local over-connectivity but long-distance disconnection. Current opinion in neurobiology 15:225-230.

Dale AM, Fischl B, Sereno MI. 1999. Cortical surface-based analysis: I. Segmentation and surface reconstruction. Neuroimage 9:179-194.

Dale AM, Sereno M. 1993. Improved localization of cortical activity by combining EEG and MEG with MRI cortical surface reconstruction: a linear approach. Journal of cognitive neuroscience 5:162-176.

Deoni SC, Williams SC, Jezzard P, Suckling J, Murphy DG, Jones DK. 2008. Standardized structural magnetic resonance imaging in multicentre studies using quantitative T1 and T2 imaging at 1.5 T. Neuroimage 40:662-671.

Dupont E, Hanganu LL, Kilb W, Hirsch S, Luhmann HJ. 2006. Rapid developmental switch in the mechanisms driving early cortical columnar networks. Nature 439:79-83.

Duque A, Krsnik Z, Kostović I, Rakic P. 2016. Secondary expansion of the transient subplate zone in the developing cerebrum of human and nonhuman primates. Proceedings of the National Academy of Sciences 113:9892-9897.

Ecker C, Andrews D, Dell'Acqua F, Daly E, Murphy C, Catani M, de Schotten MT, Baron-Cohen S, Lai M, Lombardo M. 2016. Relationship Between Cortical Gyrification, White Matter Connectivity, and Autism Spectrum Disorder. Cerebral Cortex 26:225-230.

Ecker C, Bookheimer SY, Murphy DGM. 2015. Neuroimaging in autism spectrum disorder: brain structure and function across the lifespan. The Lancet Neurology 14:1121-1134.

Ecker C, Ginestet C, Feng Y, Johnston P, Lombardo MV, Lai M-C, Suckling J, Palaniyappan L, Daly E, Murphy CM. 2013b. Brain Surface Anatomy in Adults With Autism - The Relationship Between Surface Area, Cortical Thickness, and Autistic Symptoms. JAMA psychiatry 70:59-70.

Ecker C, Ronan L, Feng Y, Daly E, Murphy C, Ginestet CE, Brammer M, Fletcher PC, Bullmore ET, Suckling J. 2013a. Intrinsic gray-matter connectivity of the brain in adults with autism spectrum disorder. Proceedings of the National Academy of Sciences 110:13222-13227.

Ecker C, Suckling J, Deoni SC, Lombardo MV, Bullmore ET, Baron-Cohen S, Catani M, Jezzard P, Barnes A, Bailey AJ, Williams SC, Murphy DGM, Consortium MA. 2012. Brain Anatomy and Its Relationship to Behavior in Adults With Autism Spectrum Disorder. Archives of General Psychiatry 69:195-209.

Fischl B, Dale AM. 2000. Measuring the thickness of the human cerebral cortex from magnetic resonance images. Proceedings of the National Academy of Sciences 97:11050-11055.

Fischl B, Sereno MI, Dale AM. 1999. Cortical surface-based analysis: II: Inflation, flattening, and a surface-based coordinate system. Neuroimage 9:195-207.

Hardan A, Muddasani S, Vemulapalli M, Keshavan M, Minshew N. 2006. An MRI study of increased cortical thickness in autism. American Journal of Psychiatry 163:1290-1292.

Hoerder-Suabedissen A, Oeschger FM, Krishnan ML, Belgard TG, Wang WZ, Lee S, Webber C, Petretto E, Edwards AD, Molnár Z. 2013. Expression profiling of mouse subplate reveals a dynamic gene network and disease association with autism and schizophrenia. Proceedings of the National Academy of Sciences 110:3555-3560.

Huguet G, Ey E, Bourgeron T. 2013. The genetic landscapes of autism spectrum disorders. Annual review of genomics and human genetics 14:191-213.

Hutsler JJ, Avino T. 2015. The Relevance of Subplate Modifications to Connectivity in the Cerebral Cortex of Individuals with Autism Spectrum Disorders. In. Recent Advances on the Modular Organization of the Cortex Springer p 201-224.

Hyde KL, Samson F, Evans AC, Mottron L. 2010. Neuroanatomical differences in brain areas implicated in perceptual and other core features of autism revealed by cortical thickness analysis and voxel-based morphometry. Human Brain Mapping 31:556-566.

Jovicich J, Czanner S, Greve D, Haley E, van der Kouwe A, Gollub R, Kennedy D, Schmitt F, Brown G, MacFall J. 2006. Reliability in multi-site structural MRI studies: effects of gradient non-linearity correction on phantom and human data. Neuroimage 30:436-443.

Just MA, Keller Ta, Malace VL, Kana RK, Varama S. 2012. Autism as a neural systems disorder: a theory of frontal-posterior underconnectivity. Neuroscience & Biobehavioral Reviews, 36:1292-1313.

Kemper TL. 2010. The neurochemical basis of autism Springer p 69-82.

Kostović I, Judaš M, Sedmak G. 2011. Developmental history of the subplate zone, subplate neurons and interstitial white matter neurons: relevance for schizophrenia. International Journal of Developmental Neuroscience 29:193-205.

Lange N, Travers BG, Bigler ED, Prigge MB, Froehlich AL, Nielsen JA, Cariello AN, Zielinski BA, Anderson JS, Fletcher PT, Alexander AA. 2015. Longitudinal volumetric brain changes in autism spectrum disorder ages 6–35 years. Autism Research. 8:82-93.

Lord C, Risi S, Lambrecht L, Cook Jr EH, Leventhal BL, DiLavore PC, Pickles A, Rutter M. 2000. The Autism Diagnostic Observation Schedule—Generic: A standard measure of social and communication deficits associated with the spectrum of autism. Journal of autism and developmental disorders 30:205-223.

Lord C, Rutter M, Couteur A. 1994. Autism Diagnostic Interview-Revised: a revised version of a diagnostic interview for caregivers of individuals with possible pervasive developmental disorders. Journal of autism and developmental disorders 24:659-685.

McConnell SK, Ghosh A, Shatz CJ. 1994. Subplate pioneers and the formation of descending connections from cerebral cortex. The Journal of neuroscience 14:1892-1907.

Nordahl CW, Dierker D, Mostafavi I, Schumann CM, Rivera SM, Amaral DG, Van Essen DC. 2007. Cortical Folding Abnormalities in Autism Revealed by Surface-Based Morphometry. The Journal of Neuroscience 27:11725-11735.

Panizzon MS, Fennema-Notestine C, Kubarych TS, Chen C-H, Eyler LT, Fischl B, Franz CE, Grant MD, Hamza S, Jak A. 2012. Genetic and environmental influences of white and gray matter signal contrast: A new phenotype for imaging genetics? NeuroImage 60:1686-1695.

Pinto D, Delaby E, Merico D, Barbosa M, Merikangas A, Klei L. 2014. Convergence of genes and cellular pathways dysregulated in autism spectrum disorders. Am J Hum Genet 94:677-694.

Rosas H, Liu A, Hersch S, Glessner M, Ferrante R, Salat D, Van Der Kouwe A, Jenkins B, Dale A, Fischl B. 2002. Regional and progressive thinning of the cortical ribbon in Huntington's disease. Neurology 58:695-701.

Salat DH, Lee SY, Van Der Kouwe A, Greve DN, Fischl B, Rosas HD. 2009. Age-associated alterations in cortical gray and white matter signal intensity and gray to white matter contrast. Neuroimage 48:21-28.

Schaer M, Ottet M-C, Scariati E, Dukes D, Franchini M, Eliez S, Glaser B. 2013. Decreased frontal gyrification correlates with altered connectivity in children with autism. Frontiers in human neuroscience 7:161-173.

Ségonne F, Dale A, Busa E, Glessner M, Salat D, Hahn H, Fischl B. 2004. A hybrid approach to the skull stripping problem in MRI. Neuroimage 22:1060-1075.

Sowell ER, Thompson PM, Leonard CM, Welcome SE, Kan E, Toga AW. 2004. Longitudinal mapping of cortical thickness and brain growth in normal children. The journal of neuroscience 24:8223-8231.

Vasung L, Lepage C, Radoš M, Pletikos M, Goldman JS, Richiardi J, Raguž, Fischi-Gómex E, Karama S, Huppi P. 2016. Quantitative and qualitative analysis of transient fetal compartments during prenatal human brain development. Frontiers in neuroanatomy 10:11.

Wechsler D. 1999. Wechsler abbreviated scale of intelligence: Psychological Corporation.

Wing L. 1997. The autistic spectrum. The lancet 350:1761-1766.

Worsley K, Andermann M, Koulis T, MacDonald D, Evans A. 1999. Detecting changes in nonisotropic images. Human brain mapping 8:98-101.

Table 1. Participant Demographics

	ASD (*n*=98, [49♂, 49♀])	Control (*n*=98, [51♂, 47♀])
London	*n*= 45, (24♂, 21♀)	*n*= 44, (25♂, 19♀)
Cambridge	*n*=53, (25♂, 28♀)	*n*= 54, (26♂, 28♀)
Age, years	26 ± 7 (18-48)	27 ± 6 (18-52)
Full-scale IQ, WASI	113 ± 12 (84-136)	116 ± 9 (93 - 137)
ADI-R social[a]	17 ± 5 (10-28)	*
ADI-R communication[a]	13 ± 4 (2-24)	*
ADI-R repetitive behavior[a]	5 ± 2 (1-10)	*
ADOS social+communication[b]	9 ± 5 (0-21)	*

Table 2. Clusters of Significant Reductions in Grey White Matter Percent Contrast and Increases in Grey Matter Intensity in ASD

Measure	Cluster	Region Labels	Hemisphere	BA(*t*max)	Vertices	Talairach x	Talairach y	Talairach z	*t*max	*p*cluster
Grey-White Matter Percent Contrast										
	1	**superior temporal gyrus**, insula, lateral orbital frontal cortex, pars orbitalis, pars triangularis, postcentral gyrus, precentral gyrus, rostral middle frontal gyrus, superior frontal gyrus	L	21	10204	47	-4	-14	-3.95	4.38 x 10-6
	2	**posterior-cingulate cortex**, isthmus-cingulate cortex, lingual gyrus, precuneus cortex	R	31	5760	7	-30	39	-3.77	2.05 x 10-5
	3	**middle temporal gyrus**, banks superior temporal sulcus, inferior temporal gyrus, superior temporal gyrus	R	21	4994	54	-11	-18	-3.87	4.48 x 10-5
	4	**middle temporal gyrus**, banks superior temporal sulcus, inferior temporal gyrus, superior temporal gyrus	L	21	4837	-53	-20	-3	-3.59	1.46 x 10-5
	5	**insula**, lateral orbital frontal cortex, pars opercularis, postcentral gyrus, precentral gyrus	L	13	4168	-27	24	-1	-3.64	1.68 x 10-3
	6	**parahippocampal gyrus**, fusiform gyrus, lingual gyrus	R	19	4053	25	-53	-2	-3.34	7.63 x 10-4
	7	**medial orbital frontal cortex**, rostral anterior cingulate cortex, superior frontal gyrus	L	11	3520	-8	25	-14	-4.13	2.14 x 10-3
	8	**fusiform gyrus**, lingual gyrus, parahippocampal gyrus	L	37	3443	-36	-42	-8	-3.26	6.62 x 10-3
	9	**posterior-cingulate cortex**, isthmus-cingulate cortex, lingual gyrus, precuneus cortex	L	23	3432	-8	-56	16	-3.33	3.92 x 10-3
	10	**supramarginal gyrus**	L	40	2466	-56	-32	27	-3.15	3.26 x 10-3
Grey Matter Signal Intensity										

1	**superior temporal gyrus**, banks superior temporal sulcus, fusiform gyrus, inferior parietal cortex, inferior temporal gyrus, insula, isthmus-cingulate cortex, lateral orbital frontal cortex, lingual gyrus, middle temporal gyrus, parahippocampal gyrus, pars triangularis, supramarginal gyrus, temporal pole	R	38	17938	35	5	-10	4.02	1.69 x 10-6
2	**superior temporal gyrus**, banks superior temporal sulcus, inferior parietal cortex, inferior temporal gyrus, middle temporal gyrus	L	21	10279	-51	-26	-2	3.31	2.86 x 10-5
3	**fusiform gyrus**, inferior temporal gyrus, isthmus-cingulate cotex, lingual gyrus, precuneus cortex	L	37	6295	-44	-40	-14	3.27	2.70 x 10-3

Table and Figure Captions

Table 1, Participant Demographics: Data expressed as mean ± standard deviation (range). There were no significant between-group differences in age or IQ, $p<0.05$ (two tailed). All participants were diagnosed using ICD-10 criteria. The (a) Autism Diagnostic Interview revised (ADI-R) was used to confirm Autism Spectrum Disorder (ASD) diagnosis. ADI-R scores were unavailable for four participants. Each of these cases reached (b) Autism Diagnostic Observation Schedule (ADOS) cut offs for "autism spectrum", for all other participants the ADOS was not used as diagnostic criteria.

Figure 1, Grey and white matter signal intensity sampling procedure: (A) Grey and white matter signal intensity sampling points are shown for one 2D coronal slice. (B) White matter intensities (WMI, red line) were sampled at an absolute distance of 1mm subjacent to the white matter surface (i.e. grey-white matter boundary). Grey matter signal intensities (GMI, blue to yellow lines) were measured at projection fractions representing a percentage of the total orthogonal distance from the white matter surface to the outer pial surface starting at the white matter surface up to 60% into the cortical sheet at 10% intervals.

Figure 2, Regions of decreased grey-to-white matter signal intensity percent contrast (GWPC) in Autism Spectrum Disorder (ASD): Individuals with ASD showed significantly decreased GWPC (RFT $p<0.5$), indicating less definition between grey and white matter, in several regions highlighted in blue including (1) the posterior cingulate cortex, (2) fronto-temporal and fronto-parietal regions, as well as (3) the bilateral fusiform and entorhinal cortex. The spatial and statistical extent of these differences was greatest when tissue intensities were sampled at the grey-white matter boundary and decreased along with increasing projection fractions (a) into the cortical sheet. See Table 2 for statistical details.

Table 2, Clusters of significant reductions in grey-white matter signal intensity percent contrast (GWPC) and increases in grey matter intensity (GMI) in Autism Spectrum Disorder (ASD): Broadmann area (BA), left (L), right (R), *Vertices* indicates the number of vertices within the cluster, t_{max} represents the maximum *t*-statistic within the cluster located at the x y z Talairach coordinates listed, $p_{cluster}$ is the cluster corrected *p* value.

Figure 3, Regional differences in grey (GMI) and white matter (WMI) signal intensities in Autism Spectrum Disorder (ASD): Individuals with ASD showed no significant differences in WMI (RFT $p<0.5$) measured at 1 mm subjacent to the grey-white matter boundary (a) nor tissue intensities measured at the boundary. Significantly increased GMI (RFT $p<0.5$) was observed across all projection fractions (b) within the cortical sheet in ASD participants. The statistical and spatial extent of these increases in GMI were most evident at the 30% projection fraction and incorporated (1) the bilateral anterior temporal lobes and the left middle temporal gyrus, (2) the right temporo-parietal junction, and (3) the bilateral fusiform and entorhinal cortex. See Table 2 for statistical details.

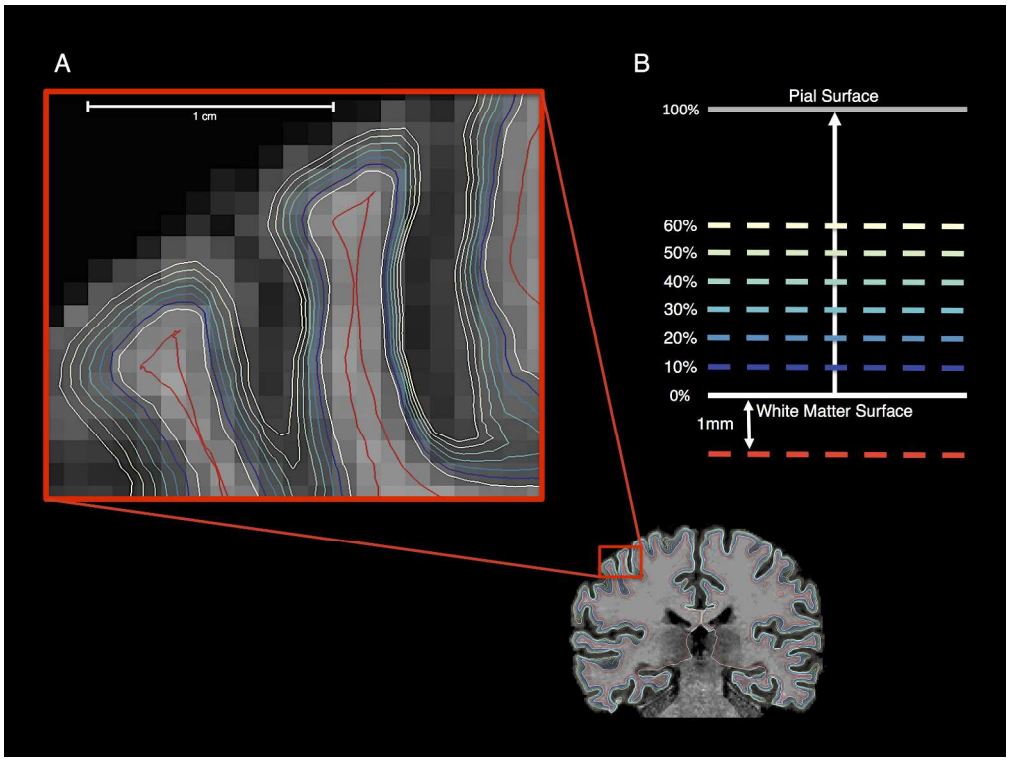

Figure 1, Grey and white matter signal intensity sampling procedure: (A) Grey and white matter signal intensity sampling points are shown for one 2D coronal slice. (B) White matter intensities (WMI, red line) were sampled at an absolute distance of 1mm subjacent to the white matter surface (i.e. grey-white matter boundary). Grey matter signal intensities (GMI, blue to yellow lines) were measured at projection fractions representing a percentage of the total orthogonal distance from the white matter surface to the outer pial surface starting at the white matter surface up to 60% into the cortical sheet at 10% intervals.

Figure 1
254x190mm (300 x 300 DPI)

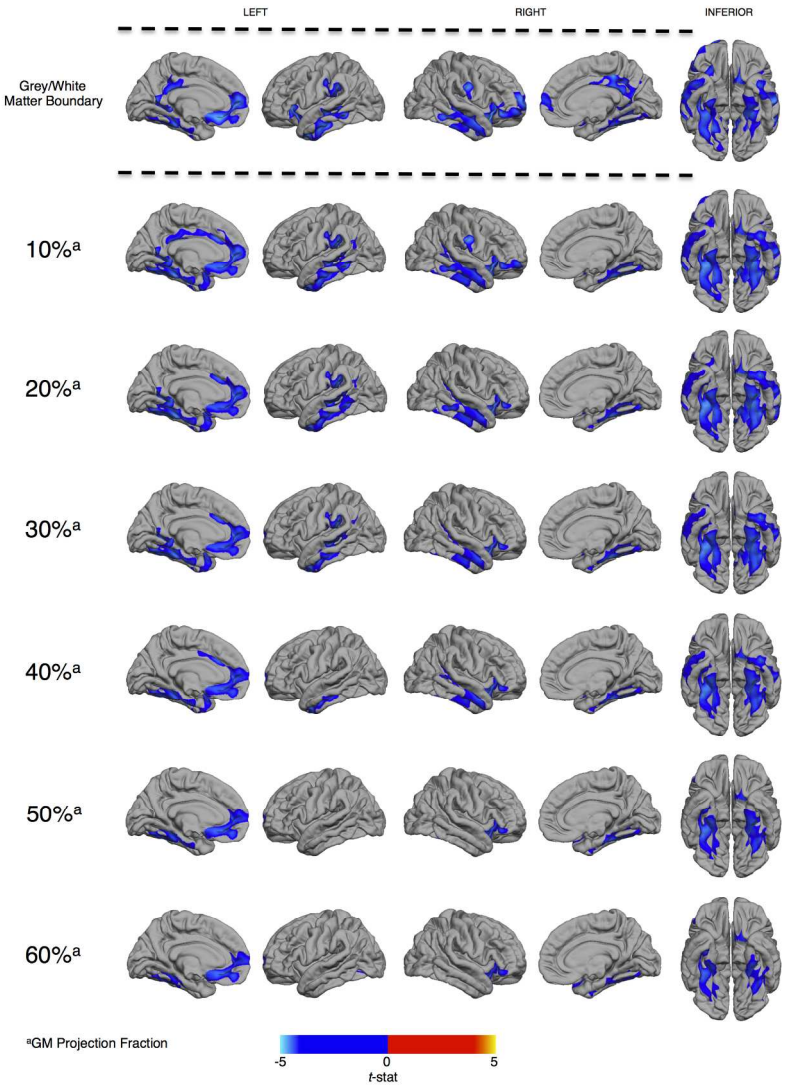

Figure 2, Regions of decreased grey-to-white matter signal intensity percent contrast (GWPC) in Autism Spectrum Disorder (ASD): Individuals with ASD showed significantly decreased GWPC (RFT $p<0.5$), indicating less definition between grey and white matter, in several regions highlighted in blue including (1) the posterior cingulate cortex, (2) fronto-temporal and fronto-parietal regions, as well as (3) the bilateral fusiform and entorhinal cortex. The spatial and statistical extent of these differences was greatest when tissue intensities were sampled at the grey-white matter boundary and decreased along with increasing projection fractions (a) into the cortical sheet. See Table 2 for statistical details.

Figure 2
190x254mm (300 x 300 DPI)

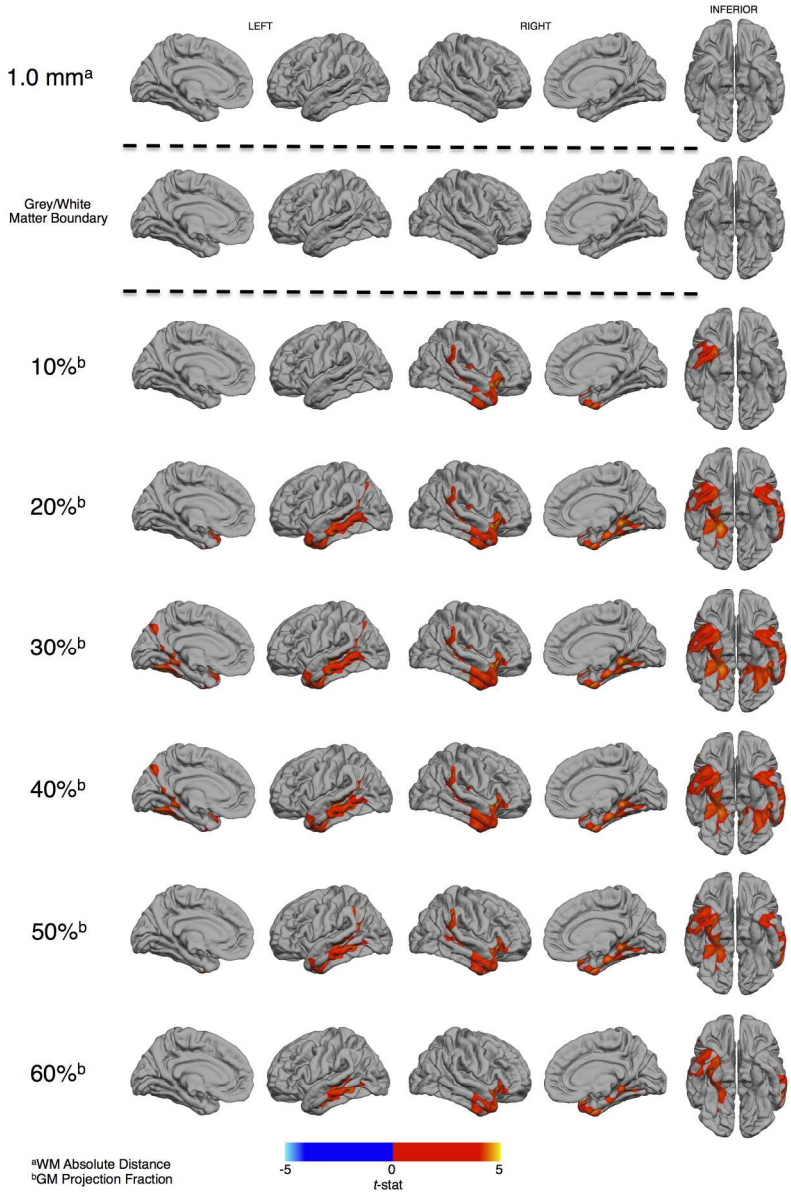

Figure 3, Regional differences in grey (GMI) and white matter (WMI) signal intensities in Autism Spectrum Disorder (ASD): Individuals with ASD showed no significant differences in WMI (RFT $p<0.5$) measured at 1 mm subjacent to the grey-white matter boundary (a) nor tissue intensities measured at the boundary. Significantly increased GMI (RFT $p<0.5$) was observed across all projection fractions (b) within the cortical sheet in ASD participants. The statistical and spatial extent of these increases in GMI were most evident at the 30% projection fraction and incorporated (1) the bilateral anterior temporal lobes and the left middle temporal gyrus, (2) the right temporo-parietal junction, and (3) the bilateral fusiform and entorhinal cortex. See Table 2 for statistical details.

Figure 3
190x254mm (300 x 300 DPI)

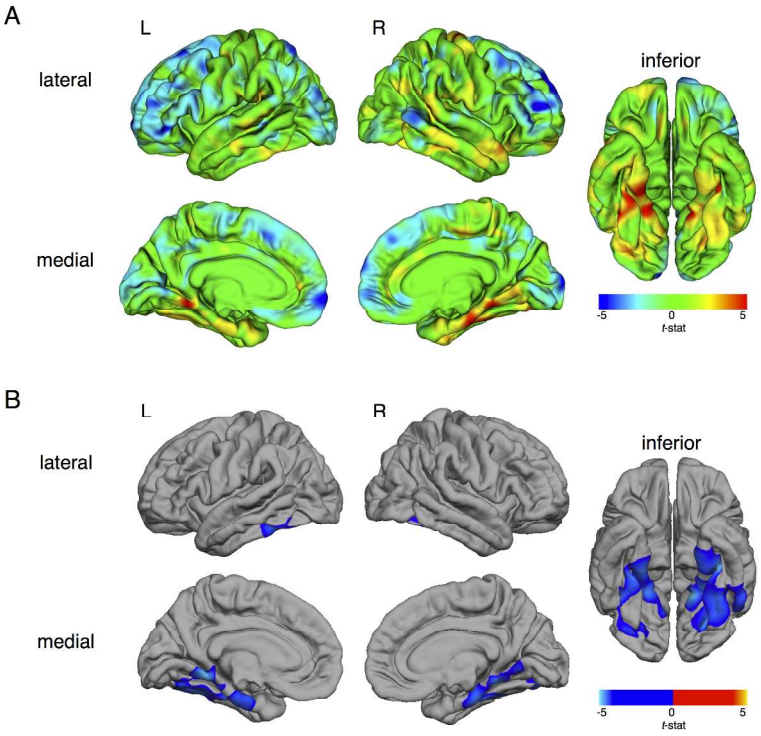

Supplementary Figure 1, Regions of decreased cortical thickness (CT) in autism spectrum disorder (ASD): A.) Between group differences in CT (uncorrected). B.) Individuals with ASD showed significantly decreased CT (RFT p<0.5) bilaterally in the parahippocampal, fusiform, and lingual gyri (highlighted in blue). See supplementary Table 1 for statistical details of these clusters.
supplementary Figure 1
254x190mm (300 x 300 DPI)

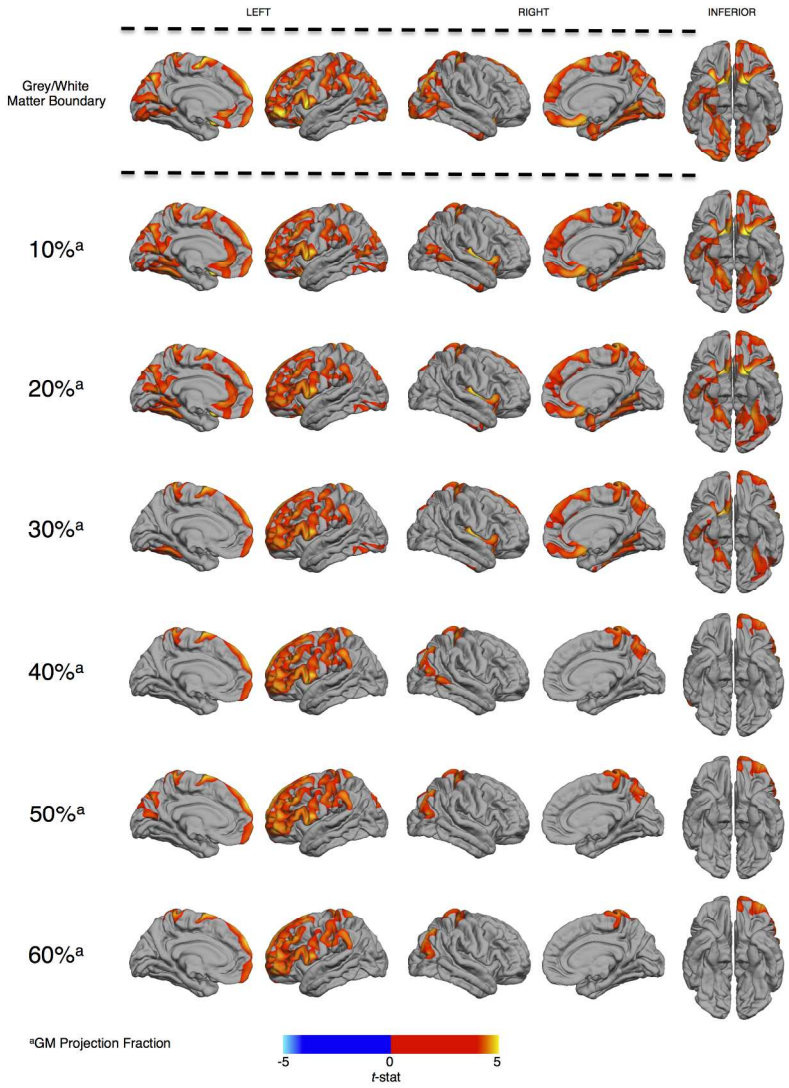

Supplementary Figure 2, Sex differences in grey-white matter signal intensity percent contrast (GWPC): Regardless of diagnosis males showed significantly greater GWPC (RFT p<0.5) compared to females across all grey matter sampling depths (a). These increases are highlighted in red and include predominantly fronto-parietal regions of the left hemisphere, and bilateral inferior temporal regions (see supplementary Table 2 for statistical details of these clusters).
supplementary Figure 2
190x254mm (300 x 300 DPI)

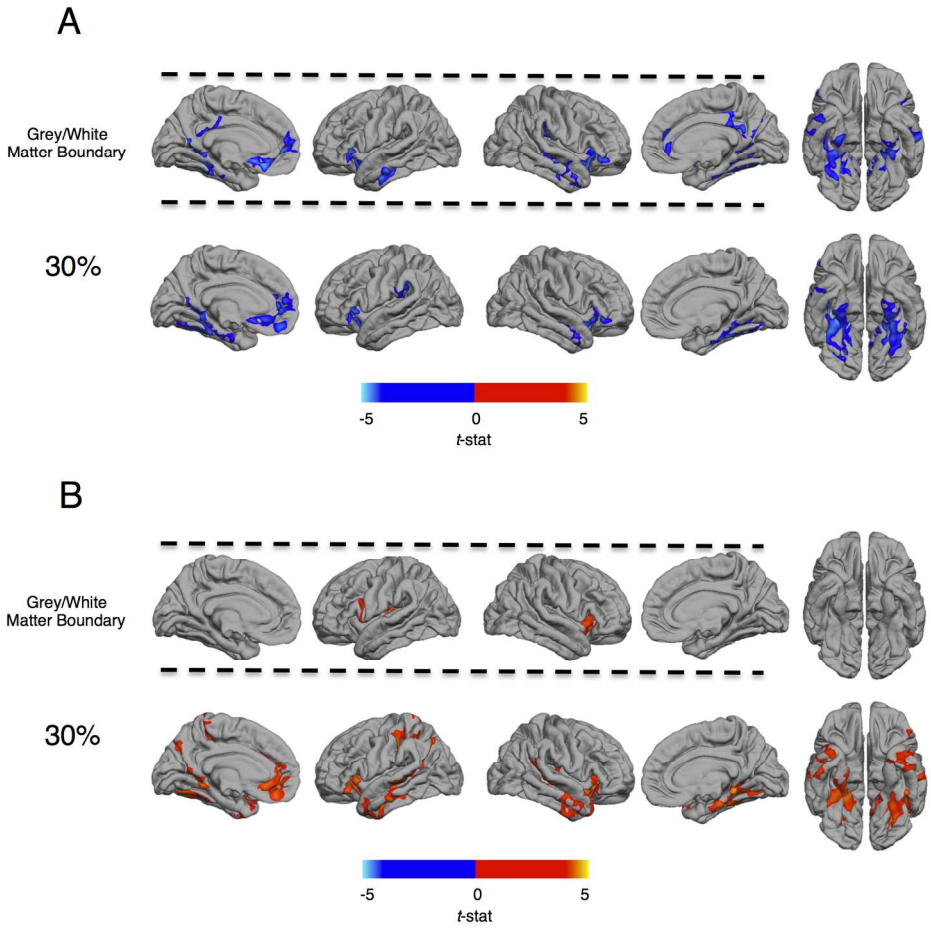

Supplementary Figure 3, Regional differences in grey-white matter signal intensity percent contrast (GWPC) and grey matter intensities (GMI) in Autism Spectrum Disorder (ASD) (5mm FWHM smoothing kernel): Between group differences in (A) GWPC and (B) GMI intensities are shown when GMI was sampled at the grey-white matter boundary (i.e. white matter surface, projection fraction 10%) and a projection fraction of 30% into the cortical sheet. Individuals with ASD showed (A) significantly decreased GWPC (RFT $p<0.5$), indicating less definition between grey and white matter, in several regions highlighted in blue. In several of these regions (B) increases in GMI, highlighted in red were also observed. These results using a 5mm FWHM smoothing kernel were largely similar to those using a 10mm FWHM smoothing kernel (Figures 2 and 3, Table 2). For statistical details of these clusters see supplementary Table 3.

Supplementary Figure 3
175x177mm (300 x 300 DPI)

Supplementary Materials

Surface deformation procedure to place the grey-white matter boundary (i.e. white matter surface)

Within this study we refer to the white matter surface (i.e. the surface that defines the transition from grey to white matter) as the grey-white matter boundary. The surface deformation procedure that places the white matter surface has previously been described by Dale et al. (1999) and is detailed bellow.

First white matter voxels are labeled through a segmentation procedure. Contiguous white matter voxels are identified through a connected components algorithm resulting in a filled white matter labeled volume. This volume is then tessellated using two triangles to define each voxel composing the surface of the white matter volume. Deformation of this "jagged" white matter tessellation to the grey-white matter boundary is accomplished by a minimization of an energy functional. The first two terms of this energy functional act to smooth the surface and regularize the tessellation by introducing a spring like property to the surface. This spring property is decomposed into two terms given as,

$$J_n = \frac{1}{2V}\left(\sum_{i=1}^{V}\sum_{j\in N_1 i}(\mathbf{n}(i)\cdot(\mathbf{x}_i-\mathbf{x}_j))^2\right)$$

$$J_t = \frac{1}{2V}\left(\sum_{i=j}^{V}\sum_{j\in N_1 i}(\mathbf{e}_0(i)\cdot(\mathbf{x}_i-\mathbf{x}_j))^2+(\mathbf{e}_1(i)\cdot(\mathbf{x}_i-\mathbf{x}_j))^2\right)$$

where $N_1(i)$ denotes the set of nearest neighbors of the i^{th} vertex, V is the total number of vertices in the tessellation, $\mathbf{n}(i)$ is the unit normal vector to the surface at the i^{th} vertex, $[\mathbf{e}_0(i),\mathbf{e}_1(i)]$ is an orthonormal basis for the tangent plane at the i^{th} retex, and $\mathbf{x}_k$ regers to the (x,y,z) position of the k^{th} vertex in the tessellation. The term J_i results in the redistribution of vertices to regions where they are needed, encouraging a uniform spacing of vertices without requiring prohibitive numbers of elements. The term J_n imposes a smoothness constraint on the surface deformation by penalizing nodes that distance themselves from the direction normal to surface from its neighboring nodes. The third term of the energy functional is based on intensity values. The volume intensity at position x_i can be written as $I(x_i)$ and this term given as,

$$J_I = \frac{1}{2V}\left(\sum_{i=1}^{V}(T(i) - I(x_i))^2\right)$$

where T(i) is the mean white matter value of border voxels within a 5mm neighborhood of each vertex, within the segmented white matter volume. The value of I(x) is computed on a subvoxel basis using trilinear interpolation. The placement of the grey-white matter boundary is achieved by minimizing an energy function that is a weighted sum of the three terms presented above,

$$J = J_t + \lambda_n J_n + \lambda_I J_I$$

where the coefficients λ_n and λ_I specify the strength of the smoothness and regularization constraints in relation to the intensity term. The gradient of this functional defines the movement of the surface tessellation such as the movement of the k^{th} vertex is given by the negative of the directional derivative with respect to $\mathbf{x}_{k,,}$

$$-\frac{\partial J}{\partial \mathbf{x}_k} = \lambda_I\big(T(k) - I(\mathbf{X}_k)\big)\nabla I(\mathbf{x}_k) + \sum_{j\in N_1(k)}(\lambda_n\big(\mathbf{n}(k)\cdot\mathbf{x}_j\big) + \mathbf{e}_0(k)\cdot\mathbf{x}_j + \mathbf{e}_1(k)\cdot\mathbf{x}_j)$$

where the volume gradient $\nabla I(\mathbf{x}_k)$ is computed using a Gaussian blurred ($\sigma = 1$) version of the MRI volume.

These automated methods for determining the grey-white matter boundary have been previously validated using scans of postmortem brains and have found FreeSurfer based measures of cortical thickness to be on average only 0.077mm different than manual measures performed on dissected tissue samples (Rosas et al. 2002). Within group systematic errors in the placement of the grey-white matter boundary using these methods would result in whole brain differences in cortical thickness that are not observed in our study. These findings thus indicate a high degree of accuracy for FreeSurfer in placing the white matter surface (i.e. the grey-white matter boundary).

Supplementary Figure Captions

Supplementary Figure 1, Regions of decreased cortical thickness (CT) in autism spectrum disorder (ASD): A.) Between group differences in CT (uncorrected). B.) Individuals with ASD showed significantly decreased CT (RFT $p<0.5$) bilaterally in the parahippocampal, fusiform, and lingual gyri (highlighted in blue). See supplementary Table 1 for statistical details of these clusters.

Supplementary Figure 2, Sex differences in grey-white matter signal intensity percent contrast (GWPC): Regardless of diagnosis males showed significantly greater GWPC (RFT $p<0.5$) compared to females across all grey matter sampling depths (a). These increases are highlighted in red and include predominantly fronto-parietal regions of the left hemisphere, and bilateral inferior temporal regions (see supplementary Table 2 for statistical details of these clusters).

Supplementary Figure 3, Regional differences in grey-white matter signal intensity percent contrast (GWPC) and grey matter intensities (GMI) in Autism Spectrum Disorder (ASD) (5mm FWHM smoothing kernel): Between group differences in (A) GWPC and (B) GMI intensities are shown when GMI was sampled at the grey-white matter boundary (i.e. white matter surface, projection fraction 10%) and a projection fraction of 30% into the cortical sheet. Individuals with ASD showed (A) significantly decreased GWPC (RFT $p<0.5$), indicating less definition between grey and white matter, in several regions highlighted in blue. In several of these regions (B) increases in GMI, highlighted in red were also observed. These results using a 5mm FWHM smoothing kernel were largely similar to those using a 10mm FWHM smoothing kernel (Figures 2 and 3, Table 2). For statistical details of these clusters see supplementary Table 3.

Supplementary Table 1

Cluster	Region Labels	Hemisphere	BA(t_{max})	No vertices	Talairach			t_{max}	$p_{cluster}$
					x	y	z		
1	parahippocampal gyrus, entorhinal cortex, fusiform gyrus, inferior temporal gyrus, lingual gyrus	L	19	6191	-17	-48	-3	-4.46	4.89 x 10-6
2	parahippocampal gyrus, fusiform gyrus, lingual gyrus	R	36	3728	21	-42	-5	-3.35	1.73 x 10-4

Supplementary Table 1, Clusters of Decreased Cortical Thickness in Autism Spectrum Disorder (ASD): Broadmann area (BA), left (L), right (R), *Vertices* indicates the number of vertices within the cluster, t_{max} represents the maximum *t*-statistic within the cluster located at the x y z Talairach coordinates listed, $p_{cluster}$ is the cluster corrected *p* value.

Supplementary Table 2

Cluster	Region Labels	Hemisphere	BA(t_{max})	No. vertices	Talairach x	Talairach y	Talairach z	t_{max}	$p_{cluster}$
1	**precentral gyrus**, frontal pole, pars opercularis, pars orbitalis, pars triangularis, rostral middle frontal gyrus, superior frontal gyrus	L	44	11867	-49	10	6	5.35	4.38×10^{-6}
2	**inferior parietal cortex**, lateral occipital cortex, lingual gyrus, middle temporal gyrus, superior parietal cortex	R	7	10199	39	-63	44	4.82	4.38×10^{-6}
3	**middle temporal gyrus**, inferior parietal cortex, lateral occipital cortex, postcentral gyrus, superior parietal cortex, supramarginal gyrus	L	19	9991	-38	-78	25	4.49	4.38×10^{-6}
4	**precuneus**, inferior temporal gyrus, isthmus-cingulate cortex, lateral occipital cortex, lingual gyrus, pericalcarine cortex, superior parietal cortex	L	7	9359	-6	-67	41	4.53	4.38×10^{-6}
5	**postcentral gyrus**, paracentral lobule, precentral gyrus, precuneus cortex, superior parietal cortex	R	3	7611	36	-30	61	4.54	4.38×10^{-6}
6	**parahippocampal gyrus**, entorhinal cortex, fusiform gyrus, inferior temporal gyrus	R	36	4001	34	-27	-15	3.42	1.16×10^{-3}
7	**lateral orbital frontal cortex**, medial orbital frontal cortex, rostral anterior cingulate cortex	L	47	3563	-24	12	-16	5.71	1.14×10^{-3}
8	**superior frontal gyrus**	R	6	3139	9	20	54	4.59	8.45×10^{-4}
9	**lateral orbital frontal cortex**, medial orbital frontal cortex	R	47	2824	26	10	-14	5.29	1.06×10^{-2}
10	**middle frontal gyrus**, precentral gyrus	L	9	2246	-37	32	25	4.31	1.81×10^{-3}
11	**paracentral lobule**, precentral gyrus, superior parietal cortex	L	6	1988	-9	-25	67	3.79	2.20×10^{-2}

Supplementary Table 2, Clusters of Increased Grey-White Matter Signal Intensity Percent Contrast (GWPC) in Males: Broadmann area (BA), left (L), right (R), *Vertices* indicates the number of vertices within the cluster, t_{max} represents the maximum *t*-statistic within the cluster located at the x y z Talairach coordinates listed, $p_{cluster}$ is the cluster corrected *p* value.

Supplementary Table 3

Measure	Cluster	Region Labels	Hemisphere	BA(*t*max)	Vertices	Talairach x	Talairach y	Talairach z	*t*max	*p*cluster
Grey-White Matter Percent Contrast										
	1	fusiform gyrus, lingual gyrus, parahippocampal gyrus	L	36	4027	-27	-39	-7	-3.66	1.33 x 10-5
	2	parahippocampal gyrus, fusiform gyrus, lingual gyrus	R	20	3447	33	-35	-18	-3.8	1.33 x 10-5
	3	medial orbital frontal cortex, rostral anterior cingulate cortex, superior frontal gyrus	L	10	2342	-10	39	-4	-3.68	1.45 x 10-5
	4	insula, lateral orbital frontal cortex	R	47	1671	26	18	-14	-4.02	1.76 x 10-4
	5	posterior-cingulate cortex, isthmus-cingulate cortex, lingual gyrus, precuneus cortex	L	30	1348	-19	-53	9	-3.72	3.52 x 10-4
	6	insula, lateral orbital frontal cortex	L	13	1267	-30	19	-2	-3.58	1.05 x 10-3
	7	middle temporal gyrus, superior temporal gyrus	R	21	1068	55	-13	-17	-3.74	1.01 x 10-2
	8	insula	L	13	1132	-38	-4	16	-2.97	4.43 x 10-2
	9	supramarginal gyrus	R	13	926	-45	-32	23	-4.13	1.24 x 10-2
Grey Matter Signal Intensity										
	1	insula, lateral orbital frontal cortex, superior temporal gyrus	R	38	4370	37	0	-12	4.01	7.28 x 10-6
	2	banks superior temporal sulcus, inferior parietal cortex, middle and superior temporal gyrus	L	21	4021	-50	-26	-2	3.64	7.89 x 10-6
	3	banks superior temporal sulcus, inferior parietal cortex, inferior, middle, and superior temporal gyri	R	41	3735	46	-36	7	2.95	1.05 x 10-5
	4	fusiform gyrus, lingual gyrus, parahippocampal gyrus	R	30	3522	18	-38	-6	3.90	7.40 x 10-6
	5	isthmus-cingulate cortex, precuneus cortex	L	29	2694	-14	-49	7	3.38	3.39 x 10-5
	6	fusiform gyrus, inferior temporal gyrus, lingual gyrus	L	19	2410	-29	-56	-3	3.56	2.22 x 10-4
	7	medial orbital frontal cortex, rostral anterior cingulate cortex, superior frontal gyrus	L	32	2165	-11	42	2	3.40	2.96 x 10-4
	8	postcentral gyrus, superior parietal cortex	L	2	1868	-46	-23	43	3.56	1.66 x 10-2
	9	insula, lateral orbital frontal cortex	L	13	1654	-30	18	-2	3.79	4.09 x 10-3
	10	paracentral lobule, superior parietal cortex,	L	5	1458	-16	-35	50	3.11	4.85 x 10-2
	11	superior temporal gyrus	L	21	1228	-45	-9	-13	2.78	2.73 x 10-2

12	inferior temporal gyrus	L	20	1085	-48	-10	-23	3.47	3.34 x 10-2	

Supplementary Table 3, Significant Reductions in Grey-White Matter Signal Intensity Percent Contrast (GWPC) and Increases in Grey Matter Intensity (GMI) in ASD (FWHM 5mm): Broadmann area (BA), left (L), right (R), *Vertices* indicates the number of vertices within the cluster, t_{max} represents the maximum *t*-statistic within the cluster located at the x y z Talairach coordinates listed, $p_{cluster}$ is the cluster corrected *p* value.